Progress In Electromagnetics Research, Vol. 126, 463–479, 2012

EFFICIENT MULTISCALE FINITE DIFFERENCE FREQUENCY DOMAIN ANALYSIS USING MULTIPLE MACROMODELS WITH COMPRESSED BOUNDARIES

J. Podwalski*, P. Kowalczyk, and M. Mrozowski

Faculty of Electronics, Telecommunications and Informatics, Gdansk University of Technology, 11/12 G. Narutowicza St., Gdansk 80-233, Poland

Abstract—In this paper, a novel idea of reducing numerical complexity of finite difference method using multiple macromodels is presented. The efficiency of the macromodeling technique depends on the number of ports of a model. To enhance the efficiency of the algorithm the field samples at the boundary of the macromodel are replaced with amplitudes of discretized Legendre polynomials. Redefining the problem in such manner results in significant reduction of the analysis time. The validity and efficiency of the proposed procedure are demonstrated by performing the analysis of two microwave filters requiring a high density mesh.

1. INTRODUCTION

The finite difference (FD) technique is one of the most versatile and simple methods of computational electromagnetics [1, 2], frequently implemented in commercial software [3, 4]. The FD method can be used to determine resonant frequencies of resonators, to investigate scattering parameters of microwave and RF devices [5, 6] and to analyze propagation characteristics of waveguides [7, 8]. However, it has several obvious disadvantages when it comes to the analysis of large and multiscale structures (i.e., containing small geometrical features in comparison to the dimension of the entire structure). In the FD method the whole domain is discretized and covered with structured Yee's mesh. In multiscale problems a huge number of variables is required to properly discretize the numerical domain. As a result, the

Received 20 January 2012, Accepted 28 February 2012, Scheduled 2 April 2012
* Corresponding author: Jakub Podwalski (jpodwal@eti.pg.gda.pl).

simulation can be very time and memory-consuming. The problem can be alleviated by applying a locally denser mesh only for crucial regions. This technique (called subgridding) is well described in the literature [9, 12, 13]. However, despite evident reduction of variables, the final problem can still be too big to analyze it in a reasonable time.

A significant improvement of the efficiency of the mentioned scheme can be achieved by applying a model order reduction (MOR) method for the subgridded regions [9–11, 14]. MOR allows one to eliminate redundant internal variables, and thus it is particularly useful when the discretization is very fine. It has been successfully applied in computational electromagnetics and photonics both for time and frequency domain analysis [12, 15–20].

Model order reduction (MOR) has originally been introduced for acceleration of numerical analysis of dynamical systems for which one evaluates the transfer function by inverting a system matrix [21]. Since 1990's numerous techniques of reduction have been developed: PVL (Pade via Lanczos) [22], PRIMA (Passive Reduced-Order Interconnect Macromodeling Algorithm) [23], ENOR (Efficient Nodal Order Reduction) [24], Quadratic Method [25], PWL (Piecewise Linear Algorithm) [26] and DEIM (Discrete Empirical Interpolation Method) [27]. All these techniques generate a small set of orthogonal vectors which span the solution subspace in the fixed frequency range. As a result, solving of the problem is limited to the new subspace.

The main idea of macromodeling procedure is quite simple [14]. At first, Maxwell's equations are transformed into Maxwell's grid equations [28]. Next, a particular region of the domain is selected, the mesh in this region is refined and input/output ports are defined. For the finite difference method, ports can be associated with the field samples at the boundary of the selected region. The global matrix operator, formed from Maxwell's grid equations, is separated into one part corresponding to the model and the second part corresponding to the rest of the domain. In the next step, a projection of the operator (its part corresponding to the model) onto a smaller subspace is performed. The projection eliminates most of the internal state variables, while the relation between the output and input ports remains preserved for a limited frequency range. Finally, the reduced part of the operator is coupled with the unprojected part of the domain. As a result, the problem size is smaller and the computation time is much shorter.

The speed of reduction and simulation depends strongly on the number of ports coupling the model with the global domain (field samples at the boundary of the model). Therefore, to improve the efficiency we propose to compress the data passed between the main

domain and the macromodel. To this end the fields at the boundary of the macromodel are expanded into a series of Legendre polynomials. As a result, a large number of ports (field samples) is reduced to several amplitudes of Legendre polynomials. Such an improvement results in a substantially smaller size of the problem and very fast analysis.

2. THE IDEA OF MACROMODELING

The concept of model order reduction for accelerating the finite difference analysis of microwave and photonic structures has been thoroughly discussed in a number of papers [9–12, 14]. For this reason only key formulas will be involved here without detailed explanation.

The finite difference method uses a discretized form of the Maxwell's equations [12]

$$\mathbf{R_H h} = j\omega \mathbf{D}_\epsilon \mathbf{e}, \tag{1}$$

$$\mathbf{R_E e} = -j\omega \mathbf{D}_\mu \mathbf{h}, \tag{2}$$

where $\mathbf{e}$ and $\mathbf{h}$ are vectors of the electric and magnetic field samples for each discretized cell. Matrices $\mathbf{R_E}$ and $\mathbf{R_H}$ are the curl matrices of vectors $\mathbf{e}$ and $\mathbf{h}$. Matrices $\mathbf{D}_\epsilon$ and $\mathbf{D}_\mu$ store the values of the permittivity and permeability for each cell.

2.1. Subgridding

In multiscale problems, where a structure to be analyzed is large and has small geometrical features, the fine mesh is required to resolve them in the FD method. This problem can be alleviated by covering the structure with a coarse mesh and introducing a technique known

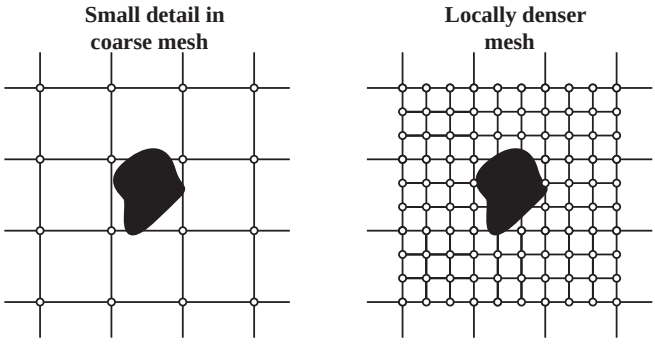

Figure 1. An example of a 2-dimensional structure with a local subgrid.

as subgridding [13] (a locally denser mesh — see Fig. 1). In such a case, Maxwell's grid equations take up the following form

$$\begin{bmatrix} \mathbf{R_H} & \mathbf{0} & \mathbf{R_{H_b}} \\ \mathbf{0} & \widehat{\mathbf{R}}_\mathbf{H} & \widehat{\mathbf{S}}_\mathbf{H} \end{bmatrix} \begin{bmatrix} \mathbf{h} \\ \widehat{\mathbf{h}} \\ \mathbf{h_b} \end{bmatrix} = s \begin{bmatrix} \mathbf{D}_\epsilon & \mathbf{0} \\ \mathbf{0} & \widehat{\mathbf{D}}_\epsilon \end{bmatrix} \begin{bmatrix} \mathbf{e} \\ \widehat{\mathbf{e}} \end{bmatrix}, \tag{3}$$

$$\begin{bmatrix} \mathbf{R_E} & \mathbf{0} \\ \mathbf{0} & \widehat{\mathbf{R}}_\mathbf{E} \\ \mathbf{R_{E_b}} & \mathbf{S_E} \end{bmatrix} \begin{bmatrix} \mathbf{e} \\ \widehat{\mathbf{e}} \end{bmatrix} = -s \begin{bmatrix} \mathbf{D}_\mu & \mathbf{0} & \mathbf{0} \\ \mathbf{0} & \widehat{\mathbf{D}}_\mu & \mathbf{0} \\ \mathbf{0} & \mathbf{0} & \mathbf{D}_{\mu_\mathbf{b}} \end{bmatrix} \begin{bmatrix} \mathbf{h} \\ \widehat{\mathbf{h}} \\ \mathbf{h_b} \end{bmatrix}, \tag{4}$$

where the symbols with and without hat refer to the dense (local) and coarse grid respectively. Additionally, vector $\mathbf{h_b}$ stores the information about the field values at the boundaries between the meshes and matrix $\mathbf{D}_{\mu_\mathbf{b}}$ stores the information about the permeability of the boundary cells.

Matrices $\mathbf{S_E}$ and $\widehat{\mathbf{S}}_\mathbf{H}$ couple the local grid $\widehat{\mathbf{e}}$ vector to boundary vector $\mathbf{h_b}$ and matrices $\mathbf{R_{E_b}}$ and $\mathbf{R_{H_b}}$ couple boundary vector $\mathbf{h_b}$ to vector $\mathbf{e}$ of the main grid.

2.2. Coupling Matrices

For a typical subgrid $\mathbf{h_b}$ stores the boundary field values explicitly. The coupling matrices in such a case are created in the following manner

$$\mathbf{R_{H_b}} = \mathbf{L_H}, \tag{5}$$

$$\mathbf{R_{E_b}} = \mathbf{B_E}, \tag{6}$$

$$\widehat{\mathbf{S}}_\mathbf{H} = \widehat{\mathbf{B}}_\mathbf{H}\mathbf{I_H}, \tag{7}$$

$$\mathbf{S_E} = \mathbf{I_E}\widehat{\mathbf{L}}_\mathbf{E}. \tag{8}$$

Matrices $\mathbf{L_H}$ and $\mathbf{B_E}$ may be regarded as the port-choosing matrices for the main grid [12]. They select the field samples defined in the coarse grid and taken at the boundary between grids (see Fig. 1). Matrices $\widehat{\mathbf{B}}_\mathbf{H}$ and $\widehat{\mathbf{L}}_\mathbf{E}$ are the port-choosing matrices of the subgrid (dense mesh), which are connected to the boundaries by interpolation matrices $\mathbf{I_H}$ and $\mathbf{I_E}$ [9].

2.3. Model Order Reduction

The region covered with a fine grid can be seen by the electromagnetic field on the main grid as a "black-box", whose electromagnetic response is given by a matrix-valued transfer function. Accordingly, the state-space equations in such region can be processed with a model order

reduction algorithm (see [14] for details). In our research we focus on the ENOR algorithm [24], which is a common method capable of solving linear problems. However, for nonlinear problems the reduction should be performed with a different MOR scheme e.g., Quadratic Method [25], PWL [26] or DEIM [27].

The ENOR algorithm produces a set of orthogonal vectors spanning the subspace with a reduced number of state variables. Let us denote by $\mathbf{V}$ the basis generated by the ENOR algorithm. Using the procedure described in [14] we may transform Equations (3)–(4) to the following form.

$$\begin{bmatrix} \mathbf{R_H}' & \mathbf{0} & \mathbf{R_{H_b}} \\ \mathbf{0} & \widehat{\mathbf{V}}^T\widehat{\mathbf{R}}_\mathbf{H} & \widehat{\mathbf{V}}^T\widehat{\mathbf{S}}'_\mathbf{H} \end{bmatrix} \begin{bmatrix} \mathbf{h} \\ \widehat{\mathbf{h}} \\ \mathbf{h_b} \end{bmatrix} = s \begin{bmatrix} \mathbf{D}_\epsilon & \mathbf{0} \\ \mathbf{0} & \widehat{\mathbf{V}}^T\widehat{\mathbf{D}}_\epsilon\widehat{\mathbf{V}} \end{bmatrix} \begin{bmatrix} \mathbf{e} \\ \widehat{\mathbf{e}}_m \end{bmatrix}, \quad (9)$$

$$\begin{bmatrix} \mathbf{R_E}' & \mathbf{0} \\ \mathbf{0} & \widehat{\mathbf{R}}_\mathbf{E}\widehat{\mathbf{V}} \\ \mathbf{R_{E_b}} & \mathbf{S_E}'\widehat{\mathbf{V}} \end{bmatrix} \begin{bmatrix} \mathbf{e} \\ \widehat{\mathbf{e}} \end{bmatrix} = -s \begin{bmatrix} \mathbf{D}_\mu & \mathbf{0} & \mathbf{0} \\ \mathbf{0} & \widehat{\mathbf{D}}_\mu & \mathbf{0} \\ \mathbf{0} & \mathbf{0} & \mathbf{D}_{\mu_\mathbf{b}} \end{bmatrix} \begin{bmatrix} \mathbf{h} \\ \widehat{\mathbf{h}} \\ \mathbf{h_b} \end{bmatrix}. \quad (10)$$

The size of the basis $\mathbf{V}$ exerts a significant impact on the numerical costs of the reduction procedure and total analysis time. The size of this basis (the number of columns in $\mathbf{V}$) is a product of the number of ports p and the model reduction order q. The reduction order determines a frequency range of the approximation and, for electrically small regions, takes rather small values — usually it is 2 or 3. Therefore, the size of $\mathbf{V}$ is determined by the number of ports (field samples at the boundary), which may be quite high.

To improve the efficiency of this technique we propose to compress the amount of data related to coupling between the macromodel and the main grid thereby achieving reduction of the number of ports. To this end, we postulate to replace the large number of field samples by a much smaller number of amplitudes of some fixed functions describing the field.

2.4. Legendre Polynomials Compression

Let us assume that function $F(x)$ describes the electric or magnetic field distribution on the normalized interval $x \in [-1, 1]$. In the FD method the field is represented by a vector of its samples $\mathbf{F} = [F(x_0), F(x_1), \ldots, F(x_{L-1})]^T$, where $x_n = \frac{2n-L}{L}$ and L is the number of samples ($n = 0, 1, \ldots, L-1$).

Compression using Legendre polynomials is based on a projection of the field onto a subspace spanned by vectors obtained from Legendre

polynomials sampled in fixed points. The projection matrix has the following form

$$\widetilde{\mathbf{Q}} = \begin{bmatrix} P_0(x_0) & P_1(x_0) & \dots & P_M(x_0) \\ P_0(x_1) & P_1(x_1) & \dots & P_M(x_1) \\ \vdots & & & \vdots \\ P_0(x_{L-1}) & P_1(x_{L-1}) & \dots & P_M(x_{L-1}) \end{bmatrix}, \tag{11}$$

where $P_m(x)$ is the Legendre polynomial of m-th order. Although Legendre polynomials are orthogonal in a continous domain, the matrix (11) consisting of samples of those polynomials is not orthogonal. However, this is not impediment as matrix $\widetilde{\mathbf{Q}}$ can easily be orthogonalized (e.g., by using the Gram-Schmidt orthogonalization or QR method). This improves the accuracy and simplifies calculations. For this reason, furtheron we assume that matrix $\mathbf{Q}$ represents an orthogonalized matrix $\widetilde{\mathbf{Q}}$.

According to above assumptions any vector $\mathbf{F}$ can now be decomposed in the following manner (this projection is exact if the number of basis vectors M is at least equal to the number of the field samples N)

$$\mathbf{F} = \mathbf{Q}\mathbf{a}, \tag{12}$$

where $\mathbf{a} = [a_0, a_1, \dots, a_{M-1}]^T$ is a vector of discretized (and orthogonalized) Legendre polynomial coefficients. Since $\mathbf{Q}$ is orthogonal ($\mathbf{Q}^{-1} = \mathbf{Q}^T$), the amplitudes can be found as

$$\mathbf{a} = \mathbf{Q}^T\mathbf{F}. \tag{13}$$

If the number of basis vectors M is smaller than the number of the field samples L, the projection on a subspace spanned by $M < L$ vectors can be treated as a compression. Obviously, a projection onto a truncated basis may result in loss of information. In order to quantify this loss, let us assume that $M < L$ and use (12) and (13) to get

$$\mathbf{F}_L = \mathbf{Q}\mathbf{Q}^T\mathbf{F} \tag{14}$$

where $\mathbf{F}_L$ is a compressed vector of field samples (spanned by discretized Legendre polynomials).

In such a case, the difference between $\mathbf{F}_L$ and $\mathbf{F}$ can be expressed in the following form

$$\mathbf{R}_F = \mathbf{F} - \mathbf{F}_L = \left(\mathbf{I} - \mathbf{Q}\mathbf{Q}^T\right)\mathbf{F}, \tag{15}$$

where $\mathbf{R}_F$ belongs to the complementary subspace. Simultaneously the vector $\mathbf{R}_F$ defines the inaccuracy of the projection.

2.5. Accuracy of the Compression

To determine the acceptable loss of accuracy caused by compression, we analyzed $\mathbf{R}_F$ with respect to the spatial frequency. Due to the numerical dispersion the FD technique requires 10 field samples per wavelength [1] to yield acceptable results. It implies that meaningful results are obtained for waveforms with low spatial frequency content. According to this assumption the maximal harmonic of the waveform is $\beta_{\max} = \frac{2\pi}{10\Delta} = \frac{\pi L}{10}$ (where $\Delta = \frac{2}{L}$ is a space discretization step). To measure the magnitude of the error produced by projecting the FD samples on a truncated basis of Legendre polynomials for functions with low spatial frequency contents, we shall evaluate the Discrete Fourier Transform (DFT) of (15) using only the Fourier terms satisfying the ten samples per wavelength criterion, i.e., $\beta \leq \beta_{\max} = \frac{\pi L}{10}$.

$$\mathbf{D} = \begin{bmatrix} e^{-j\beta_N x_0} & e^{-j\beta_{N-1} x_0} & \dots & 1 & \dots & e^{j\beta_{N-1} x_0} & e^{j\beta_N x_0} \\ e^{-j\beta_N x_1} & e^{-j\beta_{N-1} x_1} & \dots & 1 & \dots & e^{j\beta_{N-1} x_1} & e^{j\beta_N x_1} \\ \vdots & & & & & & \\ e^{-j\beta_N x_{L-1}} & e^{-j\beta_{N-1} x_{L-1}} & \dots & 1 & \dots & e^{j\beta_{N-1} x_{L-1}} & e^{j\beta_N x_{L-1}} \end{bmatrix} \quad (16)$$

where $\beta_n = n\pi$ and N is defined by the relation $\beta_N < \beta_{\max}$ ($N < \frac{L}{10}$).

The compression has no influence on the accuracy only if $\mathbf{R}_F$ belongs to the kernel of the matrix $\mathbf{D}$

$$\mathbf{D}\mathbf{R}_F = 0. \quad (17)$$

In other words, the compression is accurate, at least as far as FD results are concerned, if $\mathbf{R}_F$ does not contain any components of low spatial frequency (which, for the FD method, is in the range $0 < \beta \leq \frac{\pi L}{10}$). Hence, matrix $\mathbf{D}$ can be treated as a testing operator, which determines if a chosen function fulfils the criteria of $\beta_{\max}$ (product $\mathbf{D}\mathbf{R}_F$ should be close to zero). The expression

$$\mathbf{D}\mathbf{R}_F = \mathbf{D}\left(\mathbf{I} - \mathbf{Q}\mathbf{Q}^T\right)\mathbf{F} \quad (18)$$

represents then the inaccuracy of the compression for a fixed vector $\mathbf{F}$.

Since the norm of $||\mathbf{F}||$ is bounded and

$$||\mathbf{D}\mathbf{R}_F|| \leq ||\mathbf{D}\left(\mathbf{I} - \mathbf{Q}\mathbf{Q}^T\right)|| \, ||\mathbf{F}||, \quad (19)$$

one can measure the inaccuracy of projection for fields with a limited spatial frequency content by focusing on the following expression

$$\text{error} = ||\mathbf{D}\left(\mathbf{I} - \mathbf{Q}\mathbf{Q}^T\right)||. \quad (20)$$

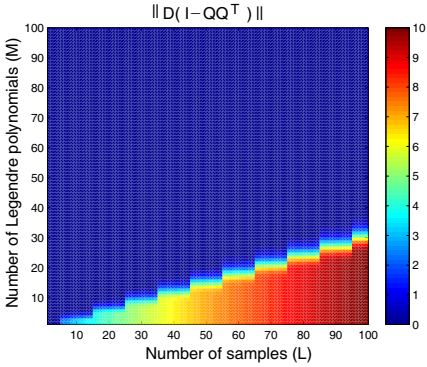

Figure 2. Error of the Legendre polynomial compression defined by expression (20) with respect to $\beta_{\max} = \frac{2\pi}{10\Delta}$ (10 samples per wavelength).

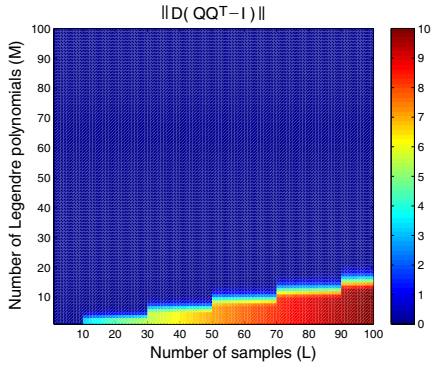

Figure 3. Error of the Legendre polynomial compression defined by expression (20) with respect to $\beta_{\max} = \frac{2\pi}{20\Delta}$ (20 samples per wavelength).

Figure 2 shows the value of (20) as a function of the number of samples and the number of Legendre polynomials. It can be seen that projection error drops, when the number of Legendre polynomials exceeds $L/3$. This means that the same spatial spectrum content of a sampled function can be faithfully represented by much fewer Legendre terms.

If the criteria for $\beta_{\max}$ is less restrictive, then, obviously, the number of polynomials can be lower (see Fig. 3 obtained for operator **D** corresponding 20 samples per wavelength).

As a final note, let us observe that other polynomials (Chebyshev, Gegenbauer or Jacobi) may also be used. The choice of Legendre polynomials was determined by their orthogonality with weight function 1.

2.6. Compression of Coupling Matrices

As explained in the previous section, it is possible to replace the field samples with a small set of amplitudes of orthogonal polynomials. Since the number of ports of the macromodel is crucial for the efficiency of the model order reduction scheme, it is reasonable to use this property to reduce this number by applying polynomial compression to the field samples at the boundary between meshes.

The compression is achieved by projection (12) and since it concerns only the fields at the boundary, it can be introduced into

the coupling matrices (5–8) in the following manner

$$\mathbf{R_{H_b}} = \mathbf{L_H Q}, \tag{21}$$

$$\mathbf{R_{E_b}} = \mathbf{Q^T B_E}, \tag{22}$$

$$\widehat{\mathbf{S}}_\mathbf{H} = \widehat{\mathbf{B}}_\mathbf{H} \mathbf{I_H Q}, \tag{23}$$

$$\mathbf{S_E} = \mathbf{Q^T I_E} \widehat{\mathbf{L}}_\mathbf{E}. \tag{24}$$

Matrices (21–24) are smaller than (5–8). This implies that the size of macromodel is also smaller. As a result, the analysis (including construction of matrix $\mathbf{V}$, using projection of boundary fields onto the Legendre polynomials) becomes more efficient.

3. NUMERICAL RESULTS

As mentioned in Subsection 2.5, the compression error drops (in the full range of spatial frequencies suitable for the FDFD mesh), when the number of Legendre polynomials reaches $L/3$. Hence, the compression level of 3 is assumed for future tests. (The compression level is defined as a ratio of the number of field samples to the number of polynomials.)

The first analyzed structure is a tunable filter composed of four metal obstacles placed in a 149.61 mm-long segment of a rectangular waveguide WR-90 [29]. A top view of the device is presented in Fig. 4. The structure is meshed with four local meshes with finer resolution defined to accurately resolve four bow-tie obstacles. Each local mesh region measures 14 by 21 mm (regions covered with gray background). The obstacles are full-height ones, therefore a 2D finite difference analysis is sufficient to solve the problem.

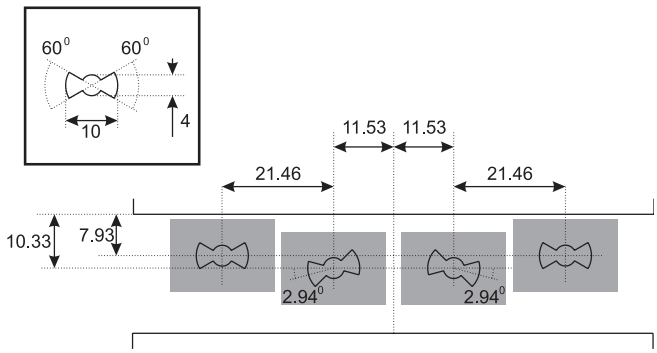

Figure 4. A top view of the filter composed of four metal obstacles placed in rectangular waveguide WR-90 (all dimensions in millimeters).

Table 1. Convergence of resonant frequencies of a few modes for different macromodel orders and different port compression level (main grid $\Delta x = 0.028\,\text{mm}$ and $\Delta y = 0.028\,\text{mm}$, refinement factor of the local meshes equal 15).

compression	order = 1	order = 2	order = 3	order = 4
21	11.3779	11.0144	11.0130	11.0130
14	11.5526	11.2356	11.2346	11.2346
8	11.5275	11.2390	11.2385	11.2385
5	11.5259	11.2393	11.2389	11.2389
4	11.5259	11.2393	11.2389	11.2389
3	11.5259	11.2393	11.2389	11.2389
1	11.5259	11.2393	11.2389	11.2389
21	11.5139	11.2536	11.2527	11.2527
14	11.5955	11.3473	11.3469	11.3469
8	11.5795	11.3516	11.3513	11.3513
5	11.5782	11.3518	11.3516	11.3516
4	11.5782	11.3519	11.3516	11.3516
3	11.5782	11.3519	11.3516	11.3516
1	11.5782	11.3519	11.3516	11.3516
21	11.8222	11.4148	11.4130	11.4130
14	11.8943	11.4621	11.4613	11.4613
8	11.8535	11.4671	11.4666	11.4666
5	11.8521	11.4672	11.4667	11.4667
4	11.8520	11.4672	11.4667	11.4667
3	11.8520	11.4672	11.4667	11.4667
1	11.8520	11.4672	11.4667	11.4667

In order to provide numerical evidence for the choice of compression level equal 3 and to determine the optimal order of macromodels, the structure was enclosed with the electric walls and the resonant frequencies were calculated. Table 1 presents the results obtained for a few selected modes for different orders of reduction and different boundary compression levels. The cell dimensions of the main grid were assumed $\Delta x = 0.028\,\text{mm}$ and $\Delta y = 0.028\,\text{mm}$ and the refinement factor of the local meshes was assumed to be 15 (the refinement factor value was determined from the previous regular FD simulations).

One can easily observe convergence of their results as a function of reduction order and compression level. Hence, for the further calculations, a choice of order 3 is reasonable and the compression level of 3 is indeed conservative. These values are used further on.

As the next step, filtering properties of the structure were examined. The analysis was performed using commercial software HFSS [30], the regular FD method ($\Delta x = 0.028\,\text{mm}$ and $\Delta y = 0.028\,\text{mm}$), the FD method with macromodels (refinement factor of 15) and the FD method with the compressed macromodels. The transmission/reflection characteristics of the 3-rd order Chebyshev filter with $-20\,\text{dB}$ return loss are shown in Fig. 5. The continuous line was obtained by using HFSS, the dotted line — by using the regular FD and the dashed line — by using compressed macromodels. All the results are in a very good agreement.

The average errors and the CPU time for different densities of the grid are collected in Table 2. The results obtained from the analysis using HFSS are compared with the ones from the regular FD, macromodeling (FD + MM) and with the ones applying Legendre compression (FD + MM + LC). The CPU time refers to the Matlab implementation and the error is evaluated from the following formula

$$ERR = \sqrt{\frac{1}{N}\sum_{i=1}^{N}\left[\left|S_{11}^{\text{HFSS}}(f_i)\right| - \left|S_{11}^{\text{our}}(f_i)\right|\right]^2}, \tag{25}$$

where $S_{11}^{\text{HFSS}}(f)$ was obtained from the HFSS whereas $S_{11}^{\text{our}}(f)$ from our simulation.

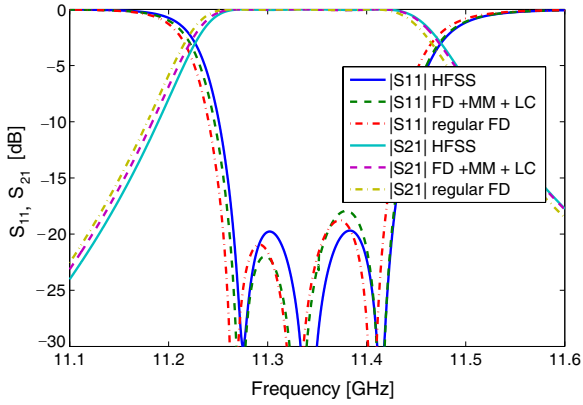

Figure 5. The 3-rd order chebyshev characteristics of the filter presented in Fig. 4.

Table 2. The average error and the calculation time per one frequency point obtained for different densities of the grid (the reduction time in brackets).

(local) grid		regular FD		FD + MM		FD + MM + LC	
Δx [mm]	Δy [mm]	error	time [s]	error	time [s]	error	time [s]
0.423	0.420	0.668	0.15	0.668	1.01 (8)	0.668	0.33 (1)
0.141	0.140	0.305	2.10	0.285	1.16 (127)	0.285	0.29 (10)
0.085	0.084	0.218	7.10	0.191	1.06 (324)	0.191	0.34 (29)
0.060	0.060	0.148	16.20	0.116	1.01 (544)	0.116	0.29 (60)
0.047	0.047	0.119	29.60	0.085	1.01 (818)	0.085	0.27 (107)
0.038	0.038	0.093	45.97	0.060	1.03 (1258)	0.060	0.35 (173)
0.033	0.032	0.074	65.18	0.039	1.02 (2253)	0.039	0.31 (234)
0.028	0.028	0.057	91.29	0.024	1.08 (2722)	0.024	0.35 (316)

Table 3. The calculation times [sec] of the frequency characteristics for 30 and 100 frequency points.

points number	regular FD	FD + MM	FD + MM + LC
30	2739	2754	327
100	9128	2830	351

In Table 3 the calculation times of the frequency characteristics are collected. It is seen that the boundary compression can significantly improve the efficiency of macromodeling. For the presented example (with 100 frequency points) the simulation time can be reduced by more than 8 times.

The second analyzed structure was a substrate integrated waveguide filter (SIW) [32, 33] whose top view is presented in Fig. 6.

This structure is particulary interesting from the point of view of macromodeling. Almost each via-hole is a separate macromodel, so in total there are 112 macromodels used in the analysis. The analysis is performed using regular FD, FD with macromodels and FD with the compressed macromodels (regions with local mesh measure 2.3×1.3 mm and are denoted with gray background). Similarly to the previous example, using Legendre polynomials at the boundaries resulted in the reduction of the number of ports of each macromodel by a factor of 3.

The results are compared with the ones obtained using the asymptotic waveform evaluation (AWE) method [31] (a continuous line in Fig. 7). The dotted line represents a regular FD analysis

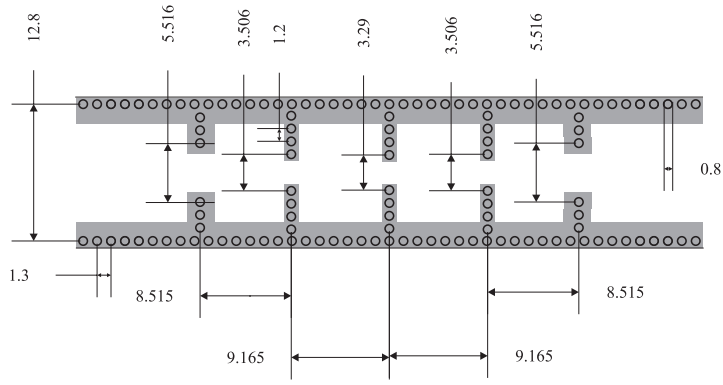

Figure 6. A top view of the analyzed SIW structure (all dimensions in millimeters).

Table 4. The average error and the calculation time per one frequency point obtained for different densities of the grid (the reduction time in brackets).

(local) grid		regular FD		FD + MM		FD + MM + LC	
Δx [mm]	Δy [mm]	error	time [s]	error	time [s]	error	time [s]
0.0571	0.0619	0.371	4.5	0.371	34.2 (39)	0.371	6.6 (25)
0.0190	0.0206	0.152	37.3	0.013	34.1 (429)	0.013	6.6 (69)
0.0114	0.0124	0.096	130.9	0.068	34.2 (1388)	0.068	6.7 (174)

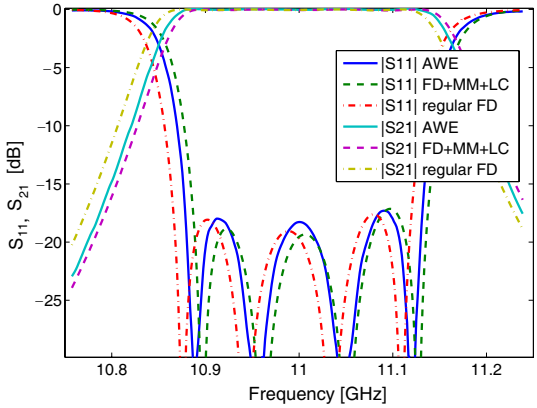

Figure 7. The 4-th order Chebyshev characteristics of the SIW filter.

($\Delta x = 0.00114\,\text{mm}$ and $\Delta y = 0.0124\,\text{mm}$) and the dashed line corresponds to the simulation using compressed macromodels (main grid: $\Delta x = 0.0571\,\text{mm}$ and $\Delta y = 0.0619\,\text{mm}$, refinement factor of 5). Also for this structure the results are in a very good agreement.

In Table 4 the results obtained from the analysis using AWE are compared with those from the regular FD, macromodeling (FD + MM) and with the ones obtained by applying Legendre compression (FD + MM + LC). The average error was evaluated by means of a formula similar to (25).

Also, for this structure a significant improvement due to compression can be observed. Moreover, it is shown that for some large problems an application of regular macromodel can be inefficient because of a huge number of ports.

4. CONCLUSIONS

The idea of compressing the ports of macromodels for finite difference method utilizing Legendre polynomials was proposed and verified on two examples. Numerical tests confirmed that the compression using Legendre polynomials yields the reduction of memory requirements and the simulation times. In all cases the improvement in memory requirements and analysis times was significant. The simulation time was reduced over 8 times for the considered examples.

It is noteworthy that the presented technique concerns macromodel boundary compression and can be applied for any MOR technique both for linear and nonlinear problems.

ACKNOWLEDGMENT

The authors would like to thank Dr. L. Kulas for his valuable assistance and support.

This work has been financed by the Polish Ministry of Science and Higher Education under the project 5407/B/T02/2010/38 "Advances in model order reduction method for multiscale problems in computational electromagnetics and photonics."

REFERENCES

1. Taflove, A. and K. R. Umashankar, "The finite-difference time-domain method for numerical modeling of electromagnetic wave interactions with arbitrary structures," *Progress In Electromagnetics Research*, Vol. 02, 287–373, 1990.
2. Xu, F., Y. Zhang, W. Hong, K. Wu, and T. J. Cui, "Finite-difference frequency-domain algorithm for modeling guided-wave properties ofsubstrate integrated waveguide," *IEEE Transactions on Microwave Theory and Techniques*, Vol. 51, No. 11, 2221–2227, Nov. 2003.
3. http://www.cst.com/.
4. http://www.qwed.com.pl/.
5. Zheng, G., B. Z. Wang, H. Li, X. F. Liu, and S. Ding, "Analysis of finite periodic dielectric gratings by the finite-difference frequency-domain method with the sub-entire-domain basis functions and wavelets," *Progress In Electromagnetics Research*, Vol. 99, 453–463, 2009.
6. Kusiek, A. and J. Mazur, "Analysis of scattering from arbitrary configuration of cylindrical objects using hybrid finite-difference mode-matching method," *Progress In Electromagnetics Research*, Vol. 97, 105–127, 2009.
7. Chang, H. W., W. C. Cheng, and S. M. Lu, "Layer-mode transparent boundary condition for the hybrid fd-fd method," *Progress In Electromagnetics Research*, Vol. 94, 175–195, 2009.
8. Chang, H. W., Y. H. Wu, and W. C. Cheng, "Hybrid fd-fd analysis of crossing waveguides by exploiting both the plus and the cross structural symmetry," *Progress In Electromagnetics Research*, Vol. 103, 217–240, 2010.
9. Kulas, L. and M. Mrozowski, "Multilevel model order reduction," *IEEE Microwave and Wireless Components Letters*, Vol. 14, No. 4, 165–167, Apr. 2004.

10. Kulas, L. and M. Mrozowski, "Reduced-order models in FDTD," *IEEE Microwave and Wireless Components Letters*, Vol. 11, No. 10, 422–424, Oct. 2001.
11. Kulas, L. and M. Mrozowski, "Reduced order models of refined Yee's cells," *IEEE Microwave and Wireless Components Letters*, Vol. 13, No. 4, 164–166, Apr. 2003.
12. Kulas, L. and M. Mrozowski, "A fast high-resolution 3-D finite-difference time-domain scheme with macromodels," *IEEE Transactions on Microwave Theory and Techniques*, Vol. 52, No. 9, 2330–2335, Sept. 2004.
13. Kulas, L. and M. Mrozowski, "Low-reflection subgridding," *IEEE Transactions on Microwave Theory and Techniques*, Vol. 53, No. 5, 1587–1592, May 2005.
14. Kulas, L. and M. Mrozowski, "Macromodels in the frequency domain analysis of microwave resonators," *IEEE Microwave and Wireless Components Letters*, Vol. 14, 94–96, 2004.
15. Podwalski, J., P. Sypek, L. Kulas, and M. Mrozowski, "FDTD analysis of EBG structures with macromodel cloning," *IEEE MTT-S International Microwave Symposium Digest*, 296–299, Jun. 11–16, 2006.
16. Cangellaris, A. C., M. Celik, S. Pasha, and Z. Li, "Electromagnetic model order reduction for system-level modeling," *IEEE Transactions on Microwave Theory and Techniques*, Vol. 47, 840–850, 1999.
17. Zhu, Y. and A. C. Cangellaris, *Multigrid Finite Element Methods for Electromagnetic Field Modeling*, John Wiley & Sons, Inc., 2006.
18. Remis, R. F., "An efficient model-order reduction approach to low-frequency transmission line modeling," *Progress In Electromagnetics Research*, Vol. 101, 139–155, 2010.
19. Kowalczyk, P., L. Kulas, and M. Mrozowski, "Analysis of microstructured optical fibers using compact macromodels," *Opt. Express*, Vol. 19, 19354–19364, 2011.
20. Song, Z., D. Su, F. Duval, and A. Louis, "Model order reduction for PEEC modeling based on moment matching," *Progress In Electromagnetics Research*, Vol. 114, 285–299, 2011.
21. Moore, B., "Principal component analysis in linear systems: Controllability, observability, and model reduction," *IEEE Trans. Automat. Contr.*, Vol. 26, 17–32, 1981.
22. Feldmann, P. and R. W. Freund, "Efficient linear circuit analysis by pade approximation via the lanczos process," *IEEE Transactions on Computer-Aided Design*, Vol. 14, 639–649, 1995.

23. Odabasioglu, A., M. Celik, and L. T. Pileggi, "PRIMA: Passive reduced-order interconnect macromodeling algorithm," *1997 IEEE/ACM International Conference on Computer-Aided Design, 1997. Digest of Technical Papers.*, 58–65, Nov. 9–13, 1997.
24. Sheehan, B. N., "ENOR: Model order reduction of RLC circuits using nodal equations for efficient factorization," *Proc. IEEE 36th Design Automat. Conf.*, 17–21, 1999.
25. Chen, Y. and J. White, "A quadratic method for nonlinear model order reduction," *Proc. Int. Conf. Modeling and Simulation of Microsystems*, 477480, 2000.
26. Rewienski, M. and J. White, "A trajectory piecewise-linear approach to model order reduction and fast simulation of nonlinear circuits and micromachined devices," *IEEE Transactions on Computer-Aided Design of Integrated Circuits and Systems*, Vol. 22, No. 2, 155–170, Feb. 2003.
27. Chaturantabut, S. and D. C. Sorensen, "Discrete empirical interpolation for nonlinear model reduction," *Proceedings of the 48th IEEE Conference on Decision and Control, 2009 held jointly with the 2009 28th Chinese Control Conference. CDC/CCC 2009*, 4316–4321, Dec. 15–18, 2009.
28. Dohlus, J. M., P. Hahne, X. Du, B. Wagner, T. Weiland, and S. G. Wipf, "Using the Maxwell grid equations to solve large problems," *IEEE Transactions on Magnetics*, Vol. 29, No. 2, 1914–1917, Mar. 1993.
29. Lech, R. and J. Mazur, "Tunable waveguide filter with bow-tie metallic posts," *IEE Proceedings — Microwaves, Antennas and Propagation*, Vol. 151, No. 2, 156–160, Apr. 2004.
30. "ANSYS HFSS," 3D Full-wave Electromagnetic Field Simulation, http://www.ansoft.com/products/hf/hfss/overview.cfm.
31. Belenguer, A., H. Esteban, E. Diaz, C. Bachiller, J. Cascon, and V. E. Boria, "Hybrid technique plus fast frequency sweep for the efficient and accurate analysis of substrate integrated waveguide devices," *IEEE Transactions on Microwave Theory and Techniques*, Vol. 59, No. 3, 552–560, Mar. 2011.
32. Zhang, X. C., Z. Y. Yu, and J. Xu, "Novel band-pass substrate integrated waveguide (SIW) filter based on complementary split ring resonators (CSRRS)," *Progress In Electromagnetics Research*, Vol. 72, 39–46, 2007.
33. Zhang, Q. L., W. Y. Yin, S. He, and L. S. Wu, "Evanescent-mode substrate integrated waveguide (SIW) filters implemented with complementary split ring resonators," *Progress In Electromagnetics Research*, Vol. 111, 419–432, 2011.